Stability of the spiral phase in the 2D extended t-J model

Valeri N. Kotov*
Institute of Theoretical Physics,
Swiss Federal Institute of Technology (EPFL),
CH-1015 Lausanne, Switzerland

Oleg P. Sushkov†
School of Physics, University of New South Wales,
Sydney 2052, Australia

We analyze the $t-t'-t''-J$ model at low doping $\delta \ll 1$ by chiral perturbation theory and show that the (1,0) spiral state is stabilized by the presence of t', t'' above critical values around $0.2J$, assuming $t/J = 3.1$. We find that the (magnon mediated) hole-hole interactions have an important effect on the region of charge stability in the space of parameters t', t'', generally increasing stability, while the stability in the magnetic sector is guaranteed by the presence of spin quantum fluctuations (order from disorder effect). These conclusions are based on perturbative analysis performed up to two loops, with very good convergence.

I. INTRODUCTION AND SUMMARY OF BASIC NOTATION

The nature of the ground state of doped quantum antiferromagnets is a central issue for the theory of correlated electrons.[1] While it is well established that arbitrary small doping destroys conventional Néel order, it is far less clear what is the structure of the emerging ground state, and how it co-exists with superconductivity. One of the early proposals made in Ref. 2, and later explored in the context of the Hubbard and the $t-J$ models,[3,4,5,6,7,8,9,10,11,12,13] was that for small doping the collinear Néel order gives way to a non-collinear spiral state. Energy is gained since the holes can hop easier in a spiral background. However it was also established that the spiral state is itself unstable with respect to long wavelength density fluctuations, i.e. has a tendency towards phase separation, signaled by a negative charge compressibility. The general problem of what states are susceptible to instabilities, such as phase separation, and what is the true ground state of the doped antiferromagnet, is enjoying a lot of current attention.[10,14,15,16,17,18,19] Some works favor, under certain conditions, inhomogeneous ground states, such as stripes, where the holes segregate into ordered structures,[14,15] whereas others argue that ultimately the ground state is uniform.[17,18]

We have recently revisited the problem of stability of the spiral state in the extended $t-t'-t''-J$ model,[13] and have found that the uniform spiral state is stable (at low doping) above certain critical values of t', t''. In addition we have shown that superconductivity is supported in the stable region. Partial motivation for this research was provided by the considerable body of evidence that (incommensurate) magnetism co-exists with superconductivity in the LSCO family.[20] Such experiments are usually interpreted in the context of stripes,[21] however the (uniform) spiral scenario is quite consistent with the majority of data, especially in the range of doping where the charge order is "fluctuating", i.e. not in the ground state. Disorder is also expected to be important in these compounds, and can be readily incorporated into the spiral state.[22]

In the present work we use chiral perturbation theory[23,24] as our main technical tool. The theory provides a rigorous perturbative treatment of long-wavelength dynamics with Goldstone quasiparticles in a system with strong interactions. The starting point is the ground state of the Heisenberg model ($t-J$ model at half filling) which incorporates all spin quantum fluctuations. The chiral perturbation theory allows a regular calculation of all physical quantities in the leading order approximation in powers of doping δ. Subleading powers of δ depend on the short-range dynamics and hence cannot be calculated without uncontrolled approximations. Therefore we cannot determine reliably what is the exact value of δ so that it is small enough to justify our calculations. However the limit $\delta \ll 1$ justifies the approach parametrically.

In our previous work[13] we concluded that the spiral state is stable in a certain region of parameters t' and t''. It was shown that the magnetic stability is due to the existence of spin quantum fluctuations (order from disorder effect). While the strong renormalization of one hole properties due to scattering with magnons was taken into account in Ref. 13, the calculation of the compressibility at finite doping (charge response) was made for free holes (zero-loop approximation), and the calculation of the magnetic response was performed in the one-loop approximation. In the present paper we extend our calculations up to two loops for both the charge and the magnetic response. The results demonstrate that perturbation theory converges very well. The main conclusion that the magnetic stability is provided by spin quantum fluctuations (order from disorder effect) remains valid in two loops, however the higher corrections are found to have an important effect on the charge stability region in the space of parameters t', t'', generally increasing stability.

We start by summarizing some results and the notation

of Ref. 13 which will be needed for our calculations. In the S=1/2 extended $t-J$ model, one allows hopping to nearest-neighbor sites (t), as well as (diagonal) next nearest-neighbors t', and next next nearest sites t'' on a 2D square lattice:

$$H = -t\sum_{\langle ij\rangle\sigma} c^\dagger_{i\sigma}c_{j\sigma} - t'\sum_{\langle ij_1\rangle\sigma} c^\dagger_{i\sigma}c_{j_1\sigma} - t''\sum_{\langle ij_2\rangle\sigma} c^\dagger_{i\sigma}c_{j_2\sigma} + J\sum_{\langle ij\rangle\sigma}\left(\mathbf{S}_i.\mathbf{S}_j - \frac{1}{4}n_in_j\right). \quad (1)$$

The $c^\dagger_{i\sigma}$ operators act in the space with no douple electron occupancy. The number of added holes, per site, is denoted by δ, and is referred to as doping. We also set the total number of sites $N=1$ and measure all the energies from now on in units of J which we set to one, while t is set to its physical value:

$$t = 3.1\ , \quad J \equiv 1. \quad (2)$$

The same-sublattice hoppings t', t'' will be considered as parameters, having in mind that in the cuprates their values are argued to be $t' \approx -0.8,\ t'' \approx 0.7$, from fits of ARPES measurements.[25,26]

The one-hole Green's function is calculated in the self-consistent Born approximation (SCBA), which produces reliable results due to the absence of low-order vertex corrections.[10,27,28] The hole dispersion minima are located at the points $\mathbf{k}_0 = (\pm\pi/2, \pm\pi/2)$, which are the centers of the four faces of the magnetic Brillouin zone (MBZ). In the vicinity of these points the dispersion is quadratic:

$$\epsilon_{\mathbf{k}} \approx \frac{\beta_1}{2}k_1^2 + \frac{\beta_2}{2}k_2^2, \quad (3)$$

where $\mathbf{k}$ is defined with respect to $\mathbf{k}_0$, and k_1 is perpendicular to the face of the MBZ, while k_2 is parallel to it. The quasiparticle residue near $\mathbf{k}_0$ is $Z_{\mathbf{k}} \approx Z_{\mathbf{k}_0} \equiv Z$. By implementing the SCBA equations numerically, we have obtained the coefficients in the following expansion, valid in the range $-1 < t' < 0$, $0 < t'' < 1$:[13]

$$\begin{aligned}\beta_1 &= 1.96 + 1.15t' + 0.06t'^2 + 2.70t'' + 0.53t''^2 + 0.50t't'',\\ \beta_2 &= 0.30 - 1.33t' - 0.19t'^2 + 2.80t'' + 1.06t''^2 - 0.14t't'',\\ Z &= 0.29 + 0.055t' + 0.195t''. \end{aligned} \quad (4)$$

Then the renormalized hole-magnon interaction is written in the long-wavelength limit, by introducing the operator $\pi_{\mathbf{q}} = \alpha_{\mathbf{q}} - \beta^\dagger_{-\mathbf{q}}$, where $\alpha_{\mathbf{q}}, \beta_{\mathbf{q}}$ are the two spin waves in a two-sublattice antiferromagnet. Calling the two sublattices "a" and "b" and introducing the corresponding (renormalized) hole operators $h_{\mathbf{k}a}, h_{\mathbf{k}b}$, we obtain the Hamiltonian describing the interactions between holes and spin waves:

$$H_{h,sw} = \sum_{\mathbf{k},\mathbf{q}} M_{\mathbf{q}}\left(h^\dagger_{\mathbf{k}+\mathbf{q}a}h_{\mathbf{k}b}\pi_{\mathbf{q}} + \text{h.c.}\right). \quad (5)$$

For simplicity from now on we refer to the renormalized (dressed) holes simply as holes. The vertex in (5) is (q_1 is perpendicular to the MBZ face):

$$M_{\mathbf{q}} = -2^{7/4}Zt\frac{q_1}{\sqrt{|\mathbf{q}|}}. \quad (6)$$

We stress that $M_{\mathbf{q}} \to 0$ at $q \to 0$ in accordance with the general Adler's relation.[24] In a spiral state the spins deviate from the Néel order, leading to lowering of the ground state energy and creation of a gap in the hole spectrum. The spiral pitch Q can be directed along the (1,1) or (1,0) direction of the lattice and is proportional to doping $Q \sim \delta$. The new hole operators ψ, φ, and the corresponding energies are:

$$\begin{pmatrix}\psi^\dagger_{\mathbf{k}}\\ \varphi^\dagger_{\mathbf{k}}\end{pmatrix} = \frac{1}{\sqrt{2}}\left(h^\dagger_{\mathbf{k}a} \mp e^{-i\mu}h^\dagger_{\mathbf{k}b}\right);\ \begin{pmatrix}\epsilon^\psi_{\mathbf{k}}\\ \epsilon^\varphi_{\mathbf{k}}\end{pmatrix} = \epsilon_{\mathbf{k}} \mp \frac{\Delta}{2}. \quad (7)$$

The spiral is a coplanar state with spins lying in a fixed plane. The arbitrary phase μ is related to the orientation of this plane, which, as we will see below, does not appear in any physical observables. The operators $\psi_{\mathbf{k}}$ and $\varphi_{\mathbf{k}}$ describe spinless fermions, and due to (7) the φ fermion band is completely empty. The gap and the Fermi energy are:

$$\Delta = \frac{2Z^2t^2}{\pi\rho_s\sqrt{\beta_1\beta_2}}\,\epsilon_F\ , \quad \epsilon_F = \frac{1}{N_p}2\pi\sqrt{\beta_1\beta_2}\,\delta. \quad (8)$$

Here $\rho_s = Z_\rho/4$, $Z_\rho = 0.72$ (S=1/2) is the renormalized spin stiffness of the undoped antiferromagnet, and N_p stands for the number of full pockets enclosed by the Fermi surface. For the (1,0) spiral $N_p = 2$, while for the 45° spiral (1,1) there is only one pocket $N_p = 1$.[13] Notice that except for the band splitting (7) which absorbs the soft mode of the doped Heisenberg antiferromagnet we assume that the dispersion (3) remains rigid under doping.

The rest of the paper is organized as follows. In Section II we analyze the charge stability of the spiral states, while Section III is devoted to the stability in the magnetic sector. The dispersion variation due to doping is discussed in Section IV. Section V contains our conclusions.

II. CHARGE RESPONSE AND CHARGE STABILITY

We now proceed to calculate the charge compressibility χ, defined as $\chi^{-1} = \partial^2 E/\partial\delta^2$, where E is the ground state energy. The two simplest contributions to the energy come from the Fermi motion of holes and from the energy gain due to the spiral formation. These two contributions are:[13]

$$E^{(0)} = \frac{1}{N_p}\left(\pi\sqrt{\beta_1\beta_2} - \frac{Z^2t^2}{\rho_s}\right)\delta^2\ . \quad (9)$$

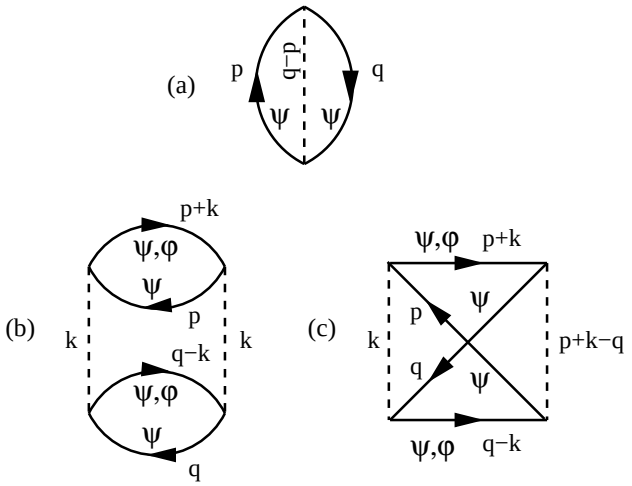

FIG. 1: (a) First order interaction energy. Dashed line represents the vertex (10). (b) Second order direct energy. (c.) Second order exchange. The labels ψ and φ show which type of fermion is present in the intermediate state.

The superscript (0) in the energy shows that interaction effects have not been taken into account (no loops). We note that the terms that are not quadratic in δ are not explicitly written, i.e. we have subtracted from the energy the constant and linear terms: $E_{AF} + \text{const.}\ \delta$.

The holes interact via spin wave exchange. Treating the hole-magnon interaction (5) in the second order of perturbation theory (the h_a, h_b operators have to be expressed via the ψ, φ operators from (7)) we obtain the effective low-energy hole-hole interaction vertex:

$$\Gamma_{\mathbf{q}} \approx -\frac{M_{\mathbf{q}}^2}{\omega_{\mathbf{q}}} = -8Z^2t^2\frac{q_1^2}{|\mathbf{q}|^2}. \tag{10}$$

Here we have neglected both the retardation effects as well as the hole energies in the denominators. This approximation should work well in the limit of low doping $\delta \ll 1$ since typical hole energies $\epsilon_{\mathbf{k}} \sim \epsilon_F \sim \delta$, while the magnon energy $\omega_{\mathbf{q}} \sim |\mathbf{q}| \sim k_F \sim \sqrt{\delta} \gg \delta$, for $\delta \ll 1$. Notice also that $Zt \approx 1$ and consequently the interaction is strong even in the long-wave-length limit.

The one-loop correction to the energy is given by the exchange diagram in Fig. 1(a). The corresponding expression reads

$$E^{(1)} = -\frac{1}{2}\sum_{\mathbf{p},\mathbf{k}} \Gamma_{\mathbf{p}-\mathbf{k}} n_{\mathbf{p}} n_{\mathbf{k}}, \tag{11}$$

where the summations are within one hole pocket enclosed by the elliptic Fermi surface, $n_{\mathbf{k}} = \theta\left(\epsilon_F - \epsilon_{\mathbf{k}}\right)$. The direct term, proportional to $\Gamma_{\mathbf{q}=\mathbf{0}}$ is set to zero, by keeping in mind the presence of a small non-zero frequency in the denominator of (10). Notice the overall sign (+) in Eq. (11) which is opposite to the sign appearing for an electron gas with Coulomb interactions. This is due to the fact that the interaction (10) is attractive.

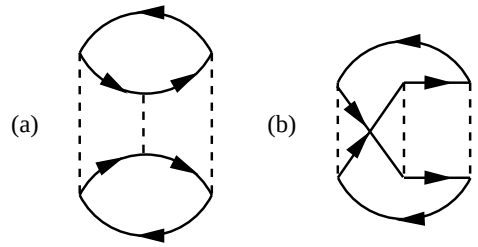

FIG. 2: Third order ladder diagrams. (a) Direct. (b.) Exchange.

Introducing the rescaled variables: $\tilde{p}_1 = p_1\sqrt{\beta_1/(2\epsilon_F)}$, $\tilde{p}_2 = p_2\sqrt{\beta_2/(2\epsilon_F)}$, we have explicitly:

$$E^{(1)} = \frac{Z^2t^2\epsilon_F^2}{\beta_1\beta_2\pi^4}\int f_{\tilde{\mathbf{p}}-\tilde{\mathbf{k}}} n_{\tilde{\mathbf{p}}} n_{\tilde{\mathbf{k}}} d^2\tilde{k} d^2\tilde{p}, \tag{12}$$

where the normalized distribution is: $n_{\tilde{\mathbf{k}}} = \theta(1 - |\tilde{\mathbf{k}}|)$, and we define the function:

$$f_{\tilde{\mathbf{k}}} = \frac{\tilde{k}_1^2}{\tilde{k}_1^2 + (\beta_1/\beta_2)\tilde{k}_2^2}. \tag{13}$$

An explicit analytical evaluation of $E^{(1)}$ is not possible, but the numerical integration in (12) does not cause any problems.

The two-loop corrections to the energy are given by the diagrams in Fig. 1(b,c), which contain both $\psi - \psi$ and $\psi - \varphi$ scatterings. The first type of contribution produces:

$$\begin{aligned} E^{(2)}_{\psi-\psi} &= \frac{1}{2}\sum_{\mathbf{p},\mathbf{k},\mathbf{q}} \frac{\Gamma_{\mathbf{k}}^2 - \Gamma_{\mathbf{k}}\Gamma_{\mathbf{p}+\mathbf{k}+\mathbf{q}}}{\epsilon^{\psi}_{\mathbf{p}} + \epsilon^{\psi}_{\mathbf{q}} - \epsilon^{\psi}_{\mathbf{p}+\mathbf{k}} - \epsilon^{\psi}_{\mathbf{q}+\mathbf{k}}} \\ &\times n_{\mathbf{p}} n_{\mathbf{q}}(1 - n_{\mathbf{p}+\mathbf{k}})(1 - n_{\mathbf{q}+\mathbf{k}}), \end{aligned} \tag{14}$$

while the second one is:

$$E^{(2)}_{\psi-\varphi} = \frac{1}{2}\sum_{\mathbf{p},\mathbf{k},\mathbf{q}} \frac{\Gamma_{\mathbf{k}}^2 - \Gamma_{\mathbf{k}}\Gamma_{\mathbf{p}+\mathbf{k}+\mathbf{q}}}{\epsilon^{\psi}_{\mathbf{p}} + \epsilon^{\psi}_{\mathbf{q}} - \epsilon^{\varphi}_{\mathbf{p}+\mathbf{k}} - \epsilon^{\varphi}_{\mathbf{q}+\mathbf{k}}} n_{\mathbf{p}} n_{\mathbf{q}}. \tag{15}$$

Here both the direct and exchange terms are added up, as shown in Fig. 1(b,c). In the rescaled variables we have the form convenient for numerical integration:

$$\begin{aligned} E^{(2)}_{\psi-\psi} &= -\frac{2Z^4t^4\epsilon_F^2}{(\beta_1\beta_2)^{3/2}\pi^6}\int [f_{\tilde{\mathbf{k}}}^2 - f_{\tilde{\mathbf{k}}} f_{\tilde{\mathbf{k}}+\tilde{\mathbf{p}}+\tilde{\mathbf{q}}}] n_{\tilde{\mathbf{p}}} n_{\tilde{\mathbf{q}}} \\ &\times (1 - n_{\tilde{\mathbf{p}}+\tilde{\mathbf{k}}})(1 - n_{\tilde{\mathbf{q}}+\tilde{\mathbf{k}}}) \frac{d^2\tilde{k} d^2\tilde{p} d^2\tilde{q}}{[\tilde{\mathbf{k}}.(\tilde{\mathbf{k}} + \tilde{\mathbf{p}} + \tilde{\mathbf{q}})]} \\ E^{(2)}_{\psi-\varphi} &= -\frac{2Z^4t^4\epsilon_F^2}{(\beta_1\beta_2)^{3/2}\pi^6}\int [f_{\tilde{\mathbf{k}}}^2 - f_{\tilde{\mathbf{k}}} f_{\tilde{\mathbf{k}}+\tilde{\mathbf{p}}+\tilde{\mathbf{q}}}] \\ &\times n_{\tilde{\mathbf{p}}} n_{\tilde{\mathbf{q}}} \frac{d^2\tilde{k} d^2\tilde{p} d^2\tilde{q}}{[\tilde{\mathbf{k}}.(\tilde{\mathbf{k}} + \tilde{\mathbf{p}} + \tilde{\mathbf{q}}) + \Delta/\epsilon_F]} \end{aligned} \tag{16}$$

Notice that the energy corrections (16) do not contain infrared or ultraviolet divergences in contrast to the 3D

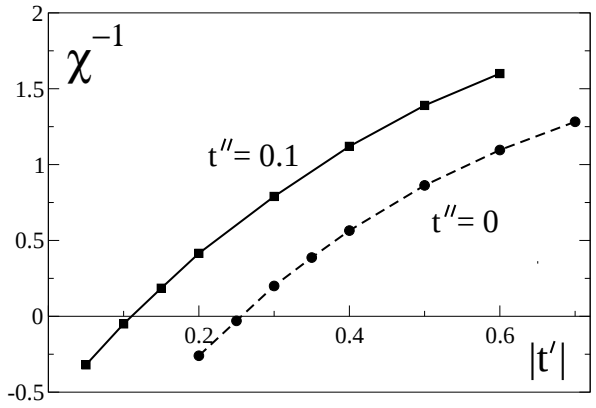

FIG. 3: The inverse compressibility χ^{-1}, as defined in Eq. (18), calculated for $t' < 0$.

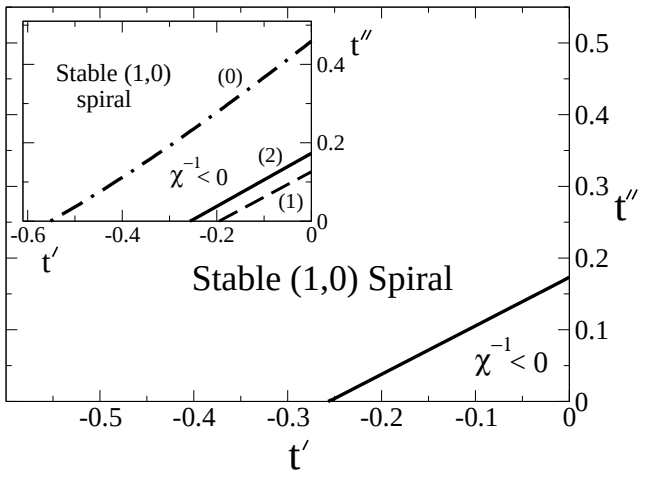

FIG. 4: Region of stability of the spiral state in the $t-t'-t''-J$ model at $t = 3.1$ (throughout the work we take $J = 1$). The unstable region, below the critical line, is marked as $\chi^{-1} < 0$. Inset: Stability boundaries calculated in different orders of perturbation theory. The dot-dashed line shows the result obtained in Ref. 13 without the interaction corrections (zero loops). The dashed line is the stability boundary calculated in the one-loop approximation ($E^{(0)}$ and $E^{(1)}$ in Eq. (17)). The solid line, which is the same in the inset and in the main figure, shows the stability line calculated in the two-loop approximation.

electron gas with Coulomb interaction.[29] In fact each of the two-loop diagrams in Fig. 1 contains an ultraviolet logarithmic divergence, $\ln\Lambda$, where $\Lambda \sim \frac{1}{\sqrt{\delta}} \gg 1$ is an ultraviolet cut-off. However the divergences are canceled out between the direct and the exchange diagrams, since the fermions ψ, φ are spinless.

In the next, third order of perturbation theory the only diagrams containing ultraviolet divergences are the "ladder" ones, shown in Fig. 2. Both diagrams separately are proportional to $\ln^2\Lambda$, and, once again, the divergences are canceled out exactly when the direct and exchange terms are added together. By examining also higher orders we find quite generally that the perturbative expansion behaves well. The absence of divergences is due to the dimensionality of the problem as well as the Goldstone nature of the mediator of the interaction.

We have verified that the hole-magnon vertex only acts within a single pocket, i.e. holes from different pockets do not interact. Thus, the total ground state energy including one and two-loop corrections is:

$$E = E^{(0)} + N_p[E^{(1)} + E^{(2)}_{\psi-\psi} + E^{(2)}_{\psi-\varphi}] \ . \qquad (17)$$

All terms in this expression are proportional to δ^2 and all the terms scale as $1/N_p$ since expressions (12) and (16) contain ϵ_F^2. Therefore, defining χ^{-1} to be the inverse compressibility of the (1,0) spiral state, i.e. $E_{(1,0)} = \frac{1}{2}\chi^{-1}\delta^2$, we have:

$$E_{(1,1)} = 2E_{(1,0)} = \chi^{-1}\delta^2 \ . \qquad (18)$$

Thus whenever the (1,0) state is lower in energy $E_{(1,0)} < E_{(1,1)}$, it is stable $\chi^{-1} > 0$, whereas the (1,1) state is always unstable, because if $E_{(1,1)} < E_{(1,0)}$ then $E_{(1,1)} < 0$ and hence $\chi^{-1}_{(1,1)} < 0$.

In Eqs. (17,18) we have neglected the contact interaction energy $E^{\rm c}$, arising from the last (density-density) term in (1), proportional to $J = 1$. In fact one could imagine adding an additional nearest neighbor Coulomb repulsion energy $V > 0$ to (1) of the form $H_V = V\sum_{\langle ij\rangle} n_i n_j$. Then the total contact energy to lowest order is: $E^{\rm c}_{(1,1)} = 0$, $E^{\rm c}_{(1,0)} = (V - 1/2)Z^2\delta^2$. The presence of the V term generally increases χ^{-1}; however as long as $V \sim 1$, the contact energy's contribution to the total energy is extremely small, since all the terms in Eq. (17) contain powers of the dominant scale $t \approx 3$.

We have found numerically that the relative importance of each successive order of perturbation theory decreases roughly by a factor of 3. For example, we estimate the first order with respect to the kinetic (Fermi motion) energy: $N_p E^{(1)}/E_F \approx 1/3$. The second-order contribution relative to the first order is also approximately: $|E^{(2)}_{\psi-\psi} + E^{(2)}_{\psi-\varphi}|/E^{(1)} \approx 1/3$. We have therefore stopped at the second order of perturbation theory and expect the contribution of the next orders to be negligible.

The inverse compressibility χ^{-1} is shown in Fig. 3 as a function of t' for two values of t''. When the point $\chi^{-1} = 0$ is reached, the system becomes unstable. The stability analysis leads us to the phase diagram of Fig. 4: the spiral phase is stable above the solid line. In Fig. 4(inset) we show the boundaries of stability calculated in different orders of perturbation theory. The dot-dashed line is the zero loop result, taking into account $E^{(0)}$ only (no interaction effects), while the dashed line is the boundary calculated in the one-loop approximation ($E^{(0)}$ and $E^{(1)}$ in Eq. (17)). Finally, the solid line is the stability border calculated in the two-loop approximation. The insert

demonstrates the good convergence of the perturbation theory. It is interesting that account of the interaction corrections (one and two-loop corrections) enlarges the region of stability in the space of parameters t', t''.

III. MAGNON STABILITY

We now proceed to verify that the region which is stable with respect to density fluctuations ($\chi^{-1} > 0$), shown in Fig. 4, is also stable in the magnetic sector. The starting point is the spin-wave Green's function:[13]

$$D_n(\omega,\mathbf{q}) = \frac{2\omega_{\mathbf{q}}\left[\omega^2 - \omega_{\mathbf{q}}^2 - 2\omega_{\mathbf{q}}P_n(\omega,\mathbf{q})\right]}{\left[\omega^2 - \omega_{\mathbf{q}}^2 - 2\omega_{\mathbf{q}}P_n(\omega,\mathbf{q})\right]^2 - 4\omega_{\mathbf{q}}^2\left|P_a(\omega,\mathbf{q})\right|^2}, \tag{19}$$

where $\omega_{\mathbf{q}} = \sqrt{2}|\mathbf{q}|$, $|\mathbf{q}| \ll 1$, is the magnon energy, and P_n, P_a are the normal and anomalous polarization operators which can be calculated perturbatively for the interaction Eq. (5). The above Green's function is the normal one (the anomalous Green's function $D_a(\omega,\mathbf{q})$ has the same denominator).

The magnetic stability requires that all the poles of (19) are at positive ω^2, i.e. no imaginary poles exist. The one loop, first order contributions to P_n, P_a were already calculated in Ref. 13, and we now calculate the second order, to match the order in the ground state energy. Due to the fact that in the spiral state the fermion operators on the two sublattices are mixed via Eq. (7), corrections to the vertex appear in lowest order. For example the second order diagrams for the normal part $P_n^{(2)}$ are shown in Fig. 5(a,b,c). After evaluating these diagrams we obtain:

$$P_n^{(2)}(0,\mathbf{q}) = \frac{M_{\mathbf{q}}^2}{4}\sum_{\mathbf{p},\mathbf{k},N_p}\Gamma_{\mathbf{p}-\mathbf{k}}\left(\frac{(n_{\mathbf{k}}-n_{\mathbf{k}+\mathbf{q}})(n_{\mathbf{p}}-n_{\mathbf{p}+\mathbf{q}})}{(\epsilon^{\psi}_{\mathbf{k}}-\epsilon^{\psi}_{\mathbf{k}+\mathbf{q}})(\epsilon^{\psi}_{\mathbf{p}}-\epsilon^{\psi}_{\mathbf{p}+\mathbf{q}})} + \frac{2n_{\mathbf{k}}n_{\mathbf{p}+\mathbf{q}}}{(\epsilon^{\psi}_{\mathbf{k}}-\epsilon^{\varphi}_{\mathbf{k}+\mathbf{q}})(\epsilon^{\psi}_{\mathbf{p}+\mathbf{q}}-\epsilon^{\varphi}_{\mathbf{p}})} - \frac{2n_{\mathbf{k}}n_{\mathbf{p}}}{(\epsilon^{\psi}_{\mathbf{k}}-\epsilon^{\varphi}_{\mathbf{k}+\mathbf{q}})(\epsilon^{\psi}_{\mathbf{p}}-\epsilon^{\varphi}_{\mathbf{p}+\mathbf{q}})}\right). \tag{20}$$

For the stability analysis one needs only the long wavelength, i.e. $|\mathbf{q}| \to 0$ limit of (20). In this limit the second and third terms (Fig. 5(b,c)) in (20) cancel out, leaving only the first term, Fig. 5(a). The corresponding diagram for the anomalous part (Fig. 5(d)) is:

$$P_a^{(2)}(0,\mathbf{q}) = -e^{-2i\mu}P_n^{(2)}(0,\mathbf{q}), \quad |\mathbf{q}| \to 0. \tag{21}$$

Adding to these results the one-loop results, $P_{n,a}^{(1)}$ from Ref. 13, we obtain the polarization operators up to two loops $P_{n,a} = P_{n,a}^{(1)} + P_{n,a}^{(2)}$. For $|\mathbf{q}| \to 0$ we have explicitly:

$$P_n(0,\mathbf{q}) = -\frac{\sqrt{2}Z^2t^2}{\pi\sqrt{\beta_1\beta_2}}\left(1+\frac{2\epsilon_F}{\Delta}\right)|\mathbf{q}| + \frac{4\sqrt{2}IZ^4t^4}{\pi^2\beta_1\beta_2}|\mathbf{q}|, \tag{22}$$

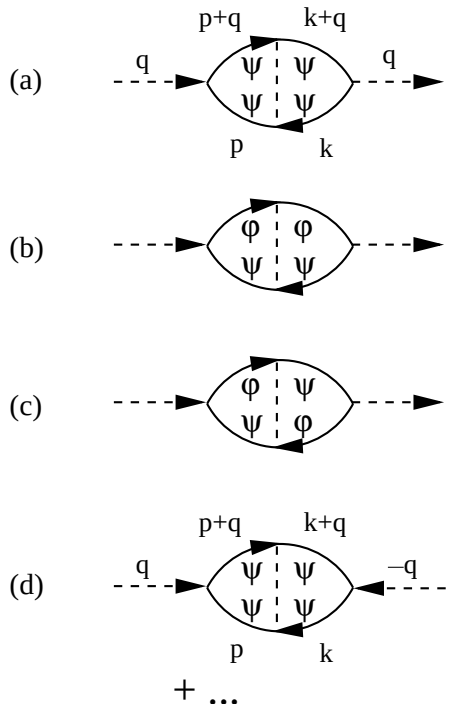

FIG. 5: (a,b,c) Two-loop, second order diagrams contributing to the normal polarization operator P_n. (d) Two-loop contributions to the anomalous polarization P_a (only first diagram of several is explicitly shown).

$$P_a(0,\mathbf{q})e^{2i\mu} = \frac{\sqrt{2}Z^2t^2}{\pi\sqrt{\beta_1\beta_2}}\left(1-\frac{2\epsilon_F}{\Delta}\right)|\mathbf{q}| - \frac{4\sqrt{2}IZ^4t^4}{\pi^2\beta_1\beta_2}|\mathbf{q}| \tag{23}$$

The quantity I is defined as:

$$I = \int_0^{2\pi}\frac{dxdy}{(2\pi)^2}\frac{(\cos x-\cos y)^2}{(\cos x-\cos y)^2+(\beta_1/\beta_2)(\sin x-\sin y)^2}. \tag{24}$$

The stability criterion reads:

$$\left[\omega_{\mathbf{q}}^2 + 2\omega_{\mathbf{q}}P_n(0,\mathbf{q})\right]^2 > 4\omega_{\mathbf{q}}^2\left|P_a(0,\mathbf{q})\right|^2, \tag{25}$$

which, for the (1,0) spiral state, is equivalent to the following inequality, in terms of the microscopic parameters:

$$\left|1-\frac{2Z^2t^2}{\pi\sqrt{\beta_1\beta_2}}-2\rho_s+\frac{8IZ^4t^4}{\pi^2\beta_1\beta_2}\right| > \left|\frac{2Z^2t^2}{\pi\sqrt{\beta_1\beta_2}}-2\rho_s-\frac{8IZ^4t^4}{\pi^2\beta_1\beta_2}\right|. \tag{26}$$

We have verified numerically that inside the region marked "Stable" in Fig. 4, the expression inside the absolute value sign on the left hand side of (26) is positive, whereas the one on the right is negative. This means that (26) is equivalent to the equation

$$1 - 4\rho_s > 0\ . \tag{27}$$

This is the same condition as the one obtained[13] in the one-loop approximation. This condition is always satisfied since $1-4\rho_s = 1-Z_\rho$, and $Z_\rho = 0.72$ due to spin quantum fluctuations renormalization in the undoped S=1/2 antiferromagnet. The physical meaning of the "quantum stabilization" is quite simple. Indeed, treating the spins semiclassically we would have $\rho_s = 1/4$ and hence a marginal ground state.[5,12,13] The spin quantum fluctuations reduce the spin stiffness and hence make the energy of the spiral state lower, see Eq. (9). This is certainly only the intuitive physical picture, while the regular proof is the one presented above, leading to Eqs. (26,27).

IV. SELF-ENERGY CORRECTIONS AND THEIR INFLUENCE ON STABILITY

The last issue we would like to address is the variation of the hole dispersion with doping and its influence on the phase diagram of Fig. 4. While the renormalization of the one-hole properties at zero doping has already been taken into account via the SCBA, Eq. (4), at finite doping the many-body hole-hole interaction corrections originating from the vertex (10) have to be calculated.

The leading self-energy diagram, contributing to the hole dispersion at finite doping is shown in Fig. 6. The corresponding expression is

$$\Sigma^{(1)}_{\mathbf{k}} = -\sum_{\mathbf{q}} \Gamma_{\mathbf{k}-\mathbf{q}} n_{\mathbf{q}} = 8Z^2t^2 \sum_{\mathbf{q}} \frac{(k_1-q_1)^2}{|\mathbf{k}-\mathbf{q}|^2} n_{\mathbf{q}} \ . \quad (28)$$

The self-energy is the same for ψ and φ fermions and therefore it influences the dispersion (3), but does not influence the gap Δ between the bands. The one-loop self-energy depends only on the momentum of the particle. We remind the reader that the one-loop self-energy is closely related to the one-loop correction to the total energy, namely by cutting a fermionic line in diagram Fig. 1(a) one obtains the self-energy Fig. 6. This means that the self-energy effect has already been taken into account in the calculation of the total energy performed in Section II. Nevertheless it is interesting to see explicitly how the dispersion changes. The integral in (28) can be easily evaluated numerically at any point of the phase diagram Fig. 4. However it is more instructive to consider the case of isotropic dispersion $\beta_1 = \beta_2 = \beta$ where the integration can be performed analytically. In this case

$$\begin{aligned} \Sigma^{(1)}_{\mathbf{k}} &= \frac{2Z^2t^2\epsilon_F}{\pi\beta}\left[1+\Omega_k(k_1^2-k_2^2)\right] \ , \\ \Omega_k &= \begin{cases} \frac{1}{2k_F^2} \ , & \text{for} \quad k<k_F \\ \frac{1}{k^2}\left(1-\frac{k_F^2}{2k^2}\right) \ , & \text{for} \quad k>k_F \ . \end{cases} \end{aligned} \quad (29)$$

With account of the self-energy the dispersion (3) should be replaced to $\epsilon_{\mathbf{k}} \to \epsilon_{\mathbf{k}} + \Sigma_{\mathbf{k}}$. Thus effectively we have a deformation of the Fermi surface

$$\beta_1 = \beta + \frac{Z^2t^2}{\pi} \ , \quad \beta_2 = \beta - \frac{Z^2t^2}{\pi} \ . \quad (30)$$

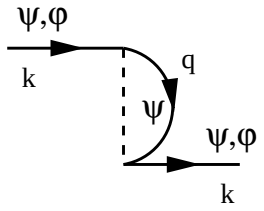

FIG. 6: One-loop self-energy correction. Dashed line represents the vertex (10). The correction is the same for ψ and φ fermions.

Notice that the deformation does not depend on the doping δ. On the other hand numerically this effect turns out to be rather weak. For the purpose of an estimate we take $t' = -0.8$, $t'' = 0.7$, corresponding to the physical values of these parameters.[25,26] At this point $\beta_1 = 2.95$, $\beta_2 = 3.80$, $Zt = 1.19$, hence the Fermi surface deformation is $\Delta\beta/\beta \approx Z^2t^2/(\pi\sqrt{\beta_1\beta_2}) \approx 0.13$.

Finally, we can summarize our findings: (i.) The leading order self-energy correction produces a weak, doping independent spectrum renormalization. (ii.) The charge stability analysis of Section II performed up to (two-loop) order $(Zt)^4$ is not influenced, at that order, by the change in the spectrum. Taking the latter effect into account produces higher order diagrams and is expected to be a very small correction, due to the previous point (i). (iii.) The magnon stability analysis of Section III is not influenced by the inclusion of (29), since the the density of states $\propto 1/\sqrt{\beta_1\beta_2}$ cancels out in the stability criterion (27).

V. CONCLUSIONS

We have studied the stability of the spiral states in the $t-t'-t''-J$ model at low doping $\delta \ll 1$. The stability was studied both in the charge and in the spin sectors, and takes into account interaction effects by including diagrams up to two loops. Our main result is that relatively small values of t', t'' are sufficient to stabilize the (1,0) spiral state, as shown in Fig. 4. For example for $t''=0$, the critical value of t' is $|t'_c/J| \approx 0.25$, or in units of t, $|t'_c| \approx 0.08t$ (for $t/J = 3.1$). The unstable region for small t', t'' is a good candidate for an inhomogeneous ground state of some sort, e.g. a striped one. Our results are also consistent with DMRG studies[30] of the extended $t-J$ model predicting a transition from stripes at $t'=0$ to a homogeneous ground state around $|t'/t| \approx 0.1$. Parameters for real cuprates correspond to the top left corner of the phase diagram Fig. 4 where the (1,0) spiral state is stable.

We have shown that the interaction effects (higher loop diagrams) should be taken into account and they tend to increase the region of spiral stability in the space of parameters t', t''. The effective coupling constant governing the perturbation theory is $g = (Zt)^2/\pi \approx 0.3$. Therefore each successive order is several times weaker

than the previous one, and thus we expect our results, calculated up to second order, to be quite reliable. The good convergence is demonstrated by the inset in Fig. 4 where we show the critical lines calculated in zero, one and two-loop orders. The magnetic stability of the spiral state is guaranteed by spin quantum fluctuations (order from disorder effect) - this conclusion remains valid in the two-loop approximation.

Our calculations are based on the chiral perturbation theory, therefore they are reliable only in the limit $\delta \ll 1$, whereas the finite doping renormalizations of the various Green's functions and vertices become more and more substantial as doping increases, leading essentially to an untreatable problem.

Acknowledgments

V.N.K. acknowledges the support of the Swiss National Fund.

* Electronic address: valeri.kotov@epfl.ch
† Electronic address: sushkov@phys.unsw.edu.au

[1] S. Sachdev, Rev. Mod. Phys. **75**, 913 (2003), and cited references.
[2] B. I. Shraiman and E. D. Siggia, Phys. Rev. Lett. **62**, 1564 (1989).
[3] C. L. Kane *et al.*, Phys. Rev. B **41**, 2653 (1990).
[4] A. Auerbach and B. E. Larson, Phys. Rev. B **43**, 7800 (1991).
[5] B. I. Shraiman and E. D. Siggia, Phys. Rev. B **46**, 8305 (1992).
[6] H. Mori and M. Hamada, Phys. Rev. B **48**, 6242 (1993).
[7] S. K. Sarker, Phys. Rev. B **47**, 2940 (1993).
[8] A. Singh, Z. Tesanovic, and J. H. Kim, Phys. Rev. B **44**, 7757 (1991).
[9] N. Dupuis, cond-mat/0105063.
[10] A. P. Kampf, Phys. Rep. **249**, 219 (1994) and references therein.
[11] C. Zhou and H. J. Schulz, Phys. Rev. B **52**, R11557 (1995).
[12] A. V. Chubukov and K. A. Musaelian, Rev. B **51**, 12605 (1995).
[13] O. P. Sushkov and V. N. Kotov, Phys. Rev. B (2004), to appear; cond-mat/0310635.
[14] S. R. White and D. J. Scalapino, Phys. Rev. B **61**, 6320 (2000).
[15] M. Vojta and S. Sachdev, Phys. Rev. Lett. **83**, 3916 (1999)
[16] L. P. Pryadko, S. Kivelson, and D. W. Hone, Phys. Rev. Lett. **80**, 5651 (1998).
[17] C. S. Hellberg and E. Manousakis, Phys. Rev. Lett. **83**, 132 (1999).
[18] M. Calandra, F. Becca, and S. Sorella, Phys. Rev. Lett. **81**, 5185 (1998).
[19] D. A. Ivanov, cond-mat/0309265.
[20] See M. -H. Julien, Physica B **329-333**, 693 (2003), for recent overview of experimental results.
[21] V. J. Emery, S. A. Kivelson, and J. M. Tranquada, Proc. Natl. Acad. Sci. USA **96**, 8814 (1999).
[22] N. Hasselmann, A. H. Castro Neto, and C. Morais Smith, Phys. Rev. B **69**, 014424 (2004).
[23] S. Weinberg, Phys. Rev. Lett. **17**, 616 (1966); Phys. Rev. **166**, 1586 (1968). See also: F. Hasenfratz and F. Niedermayer, Z. Phys. B **92**, 91 (1993) and references therein.
[24] S. L. Adler, Phys. Rev. **137**, B1022 (1965).
[25] O. K. Andersen, A. I. Liechtenstein, O. Jepsen, and F. Paulsen, J. Phys. Chem. Solids **56**, 1573 (1995).
[26] C. Kim *et al.*, Phys. Rev. Lett. **80**, 4245 (1998).
[27] S. Schmitt-Rink, C. M. Varma, and A. E. Ruckenstein, Phys. Rev. Lett. **60**, 2793 (1988).
[28] F. Marsiglio, A. E. Ruckenstein, S. Schmitt-Rink, and C. M. Varma, Phys. Rev. B **43**, 10882 (1991).
[29] M. Gell-Mann and K. A. Brueckner, Phys. Rev. **106**, 364 (1957).
[30] S. R. White and D. J. Scalapino, Phys. Rev. B **60**, R753 (1999).